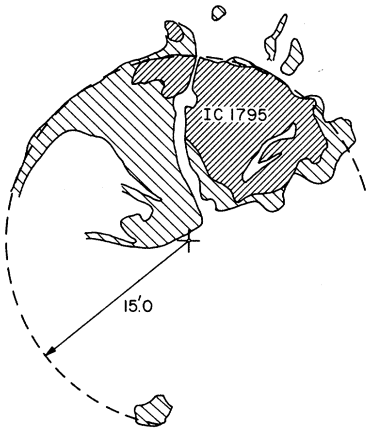

FIG. 3. Sketch of the optical field in the vicinity of the source W3C. The position of the radio source is at the cross.

and there is no sign of any emission nebula.

The source W3C is south of the emission nebula IC 1795 as already found by earlier investigations. At the actual position there is nothing visible on the Schmidt prints. This region is heavily obscured too, and it is not surprising that no identification can be made. In Fig. 3 it is shown that there might well be a relation between the OH source and a very regular arc forming the border of the most intense part of IC 1795 and continuing along fainter nebulosity. The radius of the circle with the OH source as center is 15 min of arc or 4.4 pc at a distance of 1 kpc. The true nature of this region could be obtained by mapping it in the radio continuum with a sufficiently small beam and by measuring the radial velocities of both the optical emission and the neutral hydrogen at 21-cm wavelength.

We would like to thank D. H. Rogstad for his assistance during the reduction of the data and for writing a computer program to calculate the positions. During the planning of this program Professor F. T. Haddock gave many helpful suggestions. One of us (GWR) is indebted to the Netherlands Organization for the Advancement of Pure Research for a NATO Science Fellowship.

The program of research in radio astronomy at the California Institute of Technology is supported by the U. S. Office of Naval Research under Contract No. Nonr 220(19).

[1]R. X. McGee, B. J. Robinson, F. F. Gardner, and J. G. Bolton, Nature 208, 1193 (1965).

[2]H. Weaver, D. R. W. Williams, N. H. Dieter, and W. T. Lum, Nature 208, 29 (1965).

[3]S. Weinreb, M. L. Meeks, J. C. Carter, A. H. Barrett, and A. E. E. Rogers, Nature 208, 440 (1965).

[4]B. Zuckerman, A. E. Lilley, and H. Penfield, Nature 208, 441 (1965).

[5]N. H. Dieter, H. Weaver, and D. R. W. Williams, Sky and Telescope 31, 132 (1966).

[6]A. H. Barrett and A. E. E. Rogers, Nature 210, 188 (1966).

[7]R. D. Davies, G. de Jager, and G. L. Verschuur, Nature 209, 974 (1966).

[8]N. H. Dieter, private communication.

RADIO PROPAGATION IN THE SOLAR GRAVITATIONAL FIELD

D. O. Muhleman and I. D. Johnston

Center for Radiophysics and Space Research, Cornell University, Ithaca, New York

(Received 13 June 1966)

It has been proposed by Muhleman and Reichley[1,2] and Shapiro[3] to test the general theory of relativity by measuring an additional time delay on a radar signal propagating between the earth and a target planet due to the solar gravitational field. This effect was predicted by the above authors from the Schwarzschild exterior metric and is of sufficient size to be measured with presently available planetary radar systems. However, the solar-corona electron plasma will also cause a signal delay at radio frequencies, and the question of separating the two effects is a serious one.

In this note we derive a relationship for computing the combined effect on propagation in a simple plasma in the presence of a weak gravitational field.

Møller[4] shows that Maxwell's equations in a vacuum in the presence of a static gravitational field are, in standard form,

$$\text{Curl } \vec{E} = -\frac{1}{c}\frac{\partial \vec{B}}{\partial t}, \quad \text{div } \vec{B} = 0,$$

$$\text{Curl } \vec{H} = \frac{1}{c}\frac{\partial \vec{D}}{\partial t}, \quad \text{div } \vec{D} = 4\pi\rho, \tag{1}$$

where

$$\vec{D} = \epsilon\vec{E}, \quad \vec{B} = \mu\vec{H}, \tag{2}$$

and

$$\epsilon = \mu = [1 + 2\chi/c^2]^{-1/2}. \tag{3}$$

The vector operations in Eq. (1) are defined in the generally non-Euclidean coordinates associated with the space part of the space-time metric. The scalar gravitational potential, χ, for the Schwarzschild exterior solution at a radial distance r is

$$\chi = -\alpha c^2/r, \tag{4}$$

where α is the gravitational radius for the body producing the field and is given by

$$\alpha = GM/c^2, \tag{5}$$

and where G and M are the gravitational constant and the mass of the body, respectively. For the sun, $\alpha \simeq 1.48$ km. Thus we see from Eqs. (1) and (3) that an electromagnetic wave will propagate as though it were in a medium with dielectric and magnetic constants ϵ_r and μ_r or index of refraction

$$n^2 = \epsilon_r \mu_r = [1 - 2\alpha/r]^{-1/2},$$

which is, to first order in α/r,

$$n^2 = 1 + 2\alpha/r, \tag{6}$$

a well-known result. Equation (6) represents the velocity of propagation of the electromagnetic wave but it must be realized that the wave is propagating in a curved space represented by the space part of the Schwarzschild space-time metric. In particular, the space curvature must be considered in an application of Fermat's principle utilizing the index n.[4] It can be shown, for example, that the use of Eq. (6) in a Euclidean space predicts exactly half of the total light-path curvature for starlight passing through the solar gravitational field. However, if harmonic coordinates are used[1,2,5] the formal result is obtained that the propagation can be regarded as being in a Euclidean space with index of refraction of (to first order in α/r)

$$n^2 = 1 + 4\alpha/r, \tag{6a}$$

and no further allowance for space curvature need be considered. Consequently, for the remainder of this paper we shall use Eq. (6a) in Euclidean space. No further practical considerations of the harmonic coordinates are required.

We now consider the presence of an electron plasma with density $N_e(r)$ but with no external magnetic field. Maxwell's equations become

$$\text{Curl } \vec{H} = \frac{1}{c}\epsilon_r \frac{\partial \vec{E}}{\partial t} + \frac{4\pi}{c} N_e(r) e \vec{u}, \text{ etc.,} \tag{7}$$

where $\vec{u}$ is the velocity of the electron.

The force on each electron, neglecting collisions and gravitational effects on the electron itself, and assuming that the electron is perturbed only slightly by the passage of the wave, is

$$m_e \dot{\vec{u}} = e\vec{E}. \tag{8}$$

We assume that the radar signal is monochromatic with angular frequency ω, whose time dependence is $e^{i\omega t}$. Thus

$$\vec{u} = -i(e/m_e\omega)\vec{E},$$

which upon insertion into Eq. (7) yields

$$\text{Curl } \vec{H} = \frac{\epsilon_r}{c}\left(1 - \frac{4\pi N_e(r) e^2}{\epsilon_r m_e \omega^2}\right)\frac{\partial \vec{E}}{\partial t}.$$

Consequently, to first order in α/r, the wave propagates as though it were in a medium with index of refraction

$$n^2 = 1 + \frac{4\alpha}{r} - 4\pi \frac{N_e(r) e^2}{m_e \omega^2} \tag{9}$$

if the propagation frequency is significantly greater than local plasma frequency.

The propagation delay time for the radar experiments depends, of course, on the group velocity. It can easily be shown from Eq. (9) that v_p and v_g, the phase and group velocities, respectively, are related by

$$c^2/v_p v_g = \epsilon_r \mu_r.$$

Then the total group path length between two solar-system bodies is

$$R = 2\int_1^2 (c/v_g) ds, \tag{10}$$

where the integration is along the line of the ray path which can be found by an application of Fermat's principle using the index of refraction, Eq. (9). Equation (10) then becomes

$$R = 2\int_1^2 \left[1 + \frac{2\alpha}{r} + \frac{2\pi e^2}{m_e \omega^2} N_e(r)\right] ds. \tag{11}$$

While the bending of the path due to relativity is negligible, the coronal bending must be included in computing the total delay due to the combined effects because the presence of the corona carries the ray path nearer to the sun.

Separation of coronal and relativity effects.— There are several ways to separate the effects which are experimentally feasible. The electron-density profile for the region of interest from $r = 1.3R_\odot$ to $10R_\odot$ is fairly well known from astronomical methods and is given by Allen[6] (for a quiet sun) as

$$N_e(r) = [(1.55\times10^8)/r^6]\ \mathrm{cm}^{-3}, \qquad (12)$$

where r is expressed in solar radii. The form of $N_e(r)$ is much better known than the numerical coefficient which can vary with solar activity by a factor of 2. The inverse sixth dependence, as opposed to the inverse r dependence of the general-relativistic (G.R.) term, would, in principle, allow for the determination of coronal density with a regression analysis on a sequence of observations. A far superior technique would employ simultaneous two-frequency observations for the determination of the coronal densities.

The relative importance of the two effects can be studied by approximating the ray path of integration by a straight line. With this approximation a relationship can be obtained between distance of the closest approach of the ray path to the sun, r_m, and the propagation frequency for which the G.R. delay and coronal delay are equal. The resulting curve is shown in Fig. 1. For values of r_m above the curve, the G.R. delay predominates. Thus the G.R. effect can be determined almost without regard for the corona at frequencies in the region of 10 000 Mc/sec, which is the upper frequency limit for high-power planetary radars for the forseeable future.

Finally, a more subtle technique may be developed utilizing an artificial planet. A well-known characteristic of radar reflections from natural planets is that, independently of the degree of coherence of the transmitted signal, the received signal is essentially incoherent because of the finite size and rotation of the planet. However, in the case of a space probe the reflector is replaced by a coherent range and frequency transponder. A very high degree of coherence has been demonstrated with the Mariner II and Mariner IV, for example. The

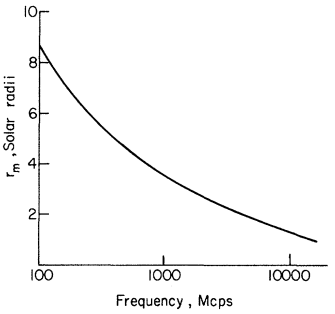

FIG. 1. Distance of closest approach for equal G.R. and coronal propagation delays against propagation frequency.

range measure to a space probe is again given by Eq. (11). However, the optical path length to the probe and back is given by

$$L = 2\int_1^2 \left[1 + \frac{2\alpha}{r} - \frac{2\pi e^2}{m_e\omega^2} N_e(r)\right] ds;$$

and the difference in the two path lengths is given by

$$\Delta = R - L = \frac{4\pi e^2}{m_e\omega^2}\int_1^2 N_e(r)ds, \qquad (13)$$

a direct measure of the integrated electron density along the ray path, independent of the G.R. effect. The optical path length cannot, of course, be measured; but the change in L with time as the ray path is swept closer to the sun owing to the orbital motion of the two bodies is observable. One simply measures the group range at time t_0 and again at time $t_0 + t_1$ while simultaneously counting the rf cycles coherently during the time interval. The difference between the two "range changes" is proportional to the derivative of Eq. (13). For purposes of this discussion we will assume that the ray path is linear, that the two planets are moving in circular orbits with radius vector $r_1 = r_\oplus = 215\ r_\odot$, and that the coronal electron density is zero at r_1. Differentiation of Eq. (13) yields for rays passing relatively close to the sun ($r_m \ll r_1$)

$$\frac{d\Delta}{dt} = \frac{\pi^{3/2}e^2}{m_e\omega^2} n \frac{\Gamma(\frac{1}{2}(n+1))}{\Gamma(\frac{1}{2}n+1)} \frac{dr_m}{dt} N_e(r_m), \qquad (13)$$

where the electron density is assumed to fall off as r^{-n} and dr_m/dt is given by the known orbital motion of the two bodies. Thus, the

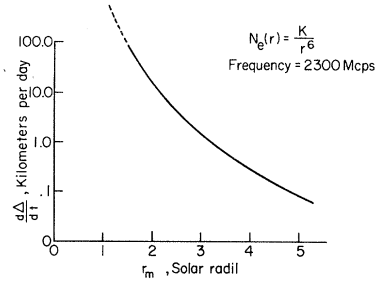

FIG. 2. Differences of group and phase delays for one-day Doppler counts against the distance of closest approach.

electron-density profile is obtained directly by this method even in regions where the G.R. effect is large compared with the coronal delay. Exact calculations would require the consideration of the path curvature; and $N_e(r_m)$ could be obtained by an iterative procedure on the equation equivalent to Eq. (13). The behavior of Eq. (13) with $n=6$ using the above assumptions and employing a frequency counting interval of one day is shown in Fig. 2. It can be shown that measurements with sufficient accuracy to demonstrate these effects are feasible utilizing the currently scheduled National Aeronautics and Space Administration deep-space probes.[7]

The Arecibo Ionospheric Observatory is operated by Cornell University with the support of the Advanced Research Projects Agency under a research contract with the U.S. Air Force Office of Scientific Research.

[1]D. O. Muhleman and P. Reichley, "Effects of General Relativity on Planetary Radar Distance Measurements," Jet Propulsion Laboratory Space Programs Summary No. 37-29, Vol. IV, 31 October 1964 (unpublished).

[2]D. O. Muhleman and P. Reichley, "General Relativistic Effects on Radar Propagation," Jet Propulsion Laboratory Space Programs Summary No. 37-31, Vol. IV, 28 February 1965 (unpublished).

[3]I. Shapiro, Phys. Rev. Letters 13, 789 (1964).

[4]C. Møller, The Theory of Relativity (Clarendon Press, Oxford, 1952).

[5]V. Fock, The Theory of Space, Time, and Gravitation (Pergamon Press, New York 1964), 2nd ed., p. 221.

[6]C. W. Allen, Monthly Notices Roy. Astron. Soc. 107, 426 (1947).

[7]D. O. Muhleman and R. M. Goldstein (unpublished).

π^+p ELASTIC DIFFERENTIAL CROSS SECTIONS FROM 2.3 to 4.0 GeV/c†

C. T. Coffin, N. Dikmen, L. Ettlinger, D. Meyer, A. Saulys, K. Terwilliger, and D. Williams
University of Michigan, Ann Arbor, Michigan
(Received 6 July 1966)

It is now known from the results of many experiments that πp scattering distributions for laboratory energies above 2 GeV have several general structural features in addition to the forward diffraction peak. In π^-p elastic scattering there is a secondary maximum or shoulder near $-t=1.2$ for all laboratory momenta between 1.6 and 12 GeV/c.[1-4] A similar secondary maximum is found in π^-p charge-exchange scattering between 2.5 and 18 GeV/c.[5,6] Finally, sharp peaks corresponding to scattering in the backward direction have been observed in both π^+- and π^--p scattering for laboratory momenta between 3.5 and 8 GeV/c.[7-9] We report here differential elastic-scattering cross sections for π^+p scattering between 2.3 and 4 GeV/c that give further information on these effects.

Our data were obtained in a spark-chamber experiment carried out at the Argonne zero-gradient synchrotron (ZGS). The apparatus and method of analysis have been described in some detail in Ref. 1, where we presented π^-p data from the same experiment. This apparatus consisted of a coplanar array of spark chambers and controlling counters surrounding a liquid-hydrogen target in such a way that all elastic events with a center-of-mass scattering angle in the interval $-0.98 \leq \cos\theta \leq 0.98$ were detected with roughly equal probability. Identification of elastic events is based on a complete reconstruction of events in three dimensions so that the constraints available are scattering angle and coplanarity. These are sufficient to reduce background from inelastic events to below 1 μb/sr in the angular region where the cross section is small.

Our results for π^+p scattering at 2.3, 2.5, 2.7, 3.0, 3.5, and 4.0 GeV/c are presented in Fig. 1 together with data near the backward direction from other experiments. The errors given for our data are purely statistical. We